Automated Analysis of EIS curves for PEM Fuel Cells using Dynamic Time Warping

M. Durand, A. Picot, J. Régnier, C. Turpin, O. Crassous, M. Scohy, R. Stephan, O. Abassie, C. Andrieux

Automated Analysis of EIS curves for PEM Fuel Cells using Dynamic Time Warping

M. Durand[1], A. Picot[1], J. Régnier[1], C. Turpin[1], O. Crassous[2], M. Scohy[2], R. Stephan[2], O. Abassie[1], and C. Andrieux[1]

***Abstract*—Fuel cell (FC) is a promising solution in order to tackle global warming problems. Though, efforts are needed for the development of reliable tools to monitor the FC state of health and to extract useful information in order to detect possible malfunctioning. The present paper propose an original method based on the Dynamic Time Warping (DTW) technique in order to process and analyze electrochemical impedance spectroscopy data. The proposed method extracts information on the similarities between 2 EIS curves. This method is evaluated on data from start-up and shut-down experimental campaign on a high temperature PEM-FC stack. Several hundreds of EIS curves are processed over 5 different conditions. The proposed method reaches 92% of correct unsupervised classifications. From the different classes identified, the ohmic resistance is extracted in order to study the impact of 2 different start-up and shut-down protocols on the FC performance.**

***Index Terms*—Dynamic Time Warping; PEM Fuel Cell; Automated Analysis; Aeronautical; Electrochemical Impedance spectroscopy; Hydrogen; Start-up and shut-down**

I. Introduction

The aeronautics industry is today driven by the prospect of a more electric aircraft incorporating efficient and environmentally-friendly technologies. In this context, Fuel Cells (*FC*) offer a number of interesting characteristics and are seen as a substitute for fossil fuel-based solutions currently used [1]. Known for years, hydrogen fuel cell technologies have been recently put again on the front of the stage with GHG emissions reduction targets. The aeronautical sector is particularly interested in greening its fleets as it still represented almost 2% of global carbon dioxide emissions in 2018, according to IEA report [2].

Recently, research efforts have intensified on a particular fuel cell technology: the high-temperature proton exchange membrane fuel cells (HT-PEM FC) which presents notably the advantages of simplified water management, higher impurities tolerance and more usable heat [3]. So that this technology can be embedded into aircraft, progress has to be made on both cost and durability. Part of the work involves understanding the origins and limiting the damage caused by the start and stop processes. In this perspective, start-up and shut-down (SU/SD) cycling aging tests have been carried out on a five-cell HT-PEM stack.

1: Université de Toulouse ; INPT, UPS ; LAPLACE (Laboratoire Plasma et Conversion d'Energie) ; ENSEEIHT, 2 rue Charles Camichel, BP 7122, F-31071 Toulouse cedex 7, France. CNRS ; LAPLACE ; F-31071 Toulouse, France. Email: name.surname@laplace.univ-tlse.fr

2: Safran Power Units, Toulouse, France.

The development of automated test benches allows repeating predefined SU/SD protocols in a reproducible manner. The evolution of the stack performances can be monitored before, during and after start and stop cycles by combining analysis of polarization curves [4], cyclic voltammetries [5] and electrochemical impedance spectroscopies (EIS) [6]. Particular attention is given to the study of EIS as this technique is feasible in operation and provides a lot of information on FC state of health and degradation behaviors.

Electrochemical Impedance Spectroscopy (EIS) is a commonly used measure to study the state of health of the FC. A small amplitude sinusoidal current excitation is imposed to the stack and its voltage response is monitored. Impedance can thus be extracted for different signal frequencies. Compared to other characterization, EIS is not much time consuming, is supposed to have a small impact on degradation and gives a lot of information about running processes.

However, the repetition of aging protocols coupled with automatic characterizations led to a large number of EIS data files raising an issue of post-processing, as aging campaign can last for several thousand hours [7]. A solution could be found thanks to shape analyzing. Information extracted from visual analysis of EIS might be difficult to transcript as one or several indicators. Dynamic Time Warping (DTW) is an algorithm that measures the similarity between 2 sequences. It has been widely used for speech processing [8], [9] and more recently for data mining [10], [11]. The present work proposes to use the DWT technique to identify the similarities between different EIS curves and use that as an indicator in order to group them by likeness in order to make the global analysis of the data easier.

The experimental test bench and PEMFC data that were used in this work are described in section II. Then, the proposed method is detailed through an example. The results obtained on the experimental data are presented and discussed in section III. Section IV concludes the paper.

II. Materials and Method

A. Experimental setup

The fuel cell used in this work consisted of a stack of five commercial PBI-based membrane-electrode assemblies (MEAs) separated by metal bipolar plates (BP) and thermally regulated around 160$\sim$180°C. The stack was designed and build by Safran Power Units. This technology is known as High Temperature Proton Exchange Membrane Fuel Cell (HT-PEMFC).

The stack temperature was dynamically regulated with a Presto A40 thermoregulator from Julabo connected to an external oil circuit. The heating and cooling phases took about 20 minutes each. To ensure the repeatability of the measures and make comparison between start or stop protocols possible, an automated control of the test bench in terms of gases flows, temperatures, pressures and currents imposed to the fuel cell was developed. Hydrogen, air and nitrogen flows were controlled and measured with mass flow controllers from Brooks. The current was imposed by two active loads, one EA-EL 9080-400 from Elektro-Automatik for the floor part, and a PBZ60-6.7 from Kikusui for dynamic excitation during EIS.

Fig. 1 displays the experimental bench with the instrumented stack in the middle. The computer that supports the HMI is on the left, in a specific tower besides the bench. This part also house the FC thermoregulator (in its bottom) as well as the electrical power management system. Other specific equipment were also used for characterizations : a Diagnostack, previously developped in collaboration with Helion, controlling the load during polarization curves and EIS plotting, and an Origalys system used for cyclic voltametry.

Figure 1. Aging test-bench for start-up & shut-down cycling.

B. Data campaign

The data used in this work are extracted from SU/SD cycling campaigns. The fuel cell is repeatedly subjected to thermal cycles to reproduce mission stresses. On start-up, when a sufficient temperature is reached, current is progressively imposed. A wait for thermal stabilization under constant flows and current conditions is then done. When stability is achieved, measurements are taken to monitor performance trends. Once data are collected, the FC is turned off by gradually reducing the current before flushing the electrodes with nitrogen or air depending on the protocol chosen.

Two different SU/SD protocols were tested: $P1$ and $P2$. On one hand, $P1$ is a laboratory-oriented SU/SD protocol with no specific constraint developed to minimize the impact of SU/SD on the FC. On the other hand, $P2$ was designed in collaboration with Safran Power Units in respect with FC industrial constraints.

In order to confirm the observation of degradations by limiting the impact of singularities, each protocol combination was repeated 50 times in a row. Before and after each of these cycling block, the fuel cell was characterized specifically by cyclic voltammetry cell by cell and a polarization curve was plotted. These performance curves were voluntary limited in the current density range explored in order to lessen the impact of charcterization itself on aging. Each time, six points were taken from 0.1 to 0.6 A/cm^2. It was also decided to only carry out these measurements between cycles of 50 repeated start-stops.

Parallel to this observation, in-operation measurements could be carried out using electrochemical impedance spectroscopy (EIS): a small amplitude sinusoidal excitation is over-imposed on current and the stack voltage response is acquired. For different sinusoidal frequencies it is then possible to plot the real and imaginary parts of the fuel cell impedance. In this study, a constant excitation amplitude of 0.77 A peak-to-peak was used. The spectrum of frequencies explored extendend from 5 kHz to 0.1 Hz. These plots reveal information on fuel cell performances and state of health during start-stop cycling. Among extractable indicators, the high frequency resistance, defined as the first intersection of the impedance plot with the real axis on a Nyquist diagram, characterizes the performances in terms of electrical charge transfer (either positive or negative). Monitoring this parameter thus reveals information on fuel cell performances and state of health during start-stop cycling. Those data can also be used for model fitting in order to improve our understanding of aging phenomena.

Please note that EIS were carried out automatically every 5 minutes as current could be imposed to the stack. This led to variability in operation conditions between characterizations even if the same conditions were achieved at the end of stabilization step. Thus, the data from each protocol can be divided into 2 classes: stabilized PXs and unstabilized PXu, where X is the protocol number. Moreover, the data from the break-in phase (BI) were kept in the dataset. A total of 383 EIS curves is obtained. The number of curves in each condition is summed up in table I.

Table I
NUMBER OF EIS CURVES IN EACH CONDITION.

BI	P1u	P1s	P2u	P2s
33	67	108	64	111

Added to the large number of starts and stops studied, a solution had to be developed in order to automatically process the data of the hundreds of EIS carried out. Thus the purpose of this work consists of separating the numerous EIS curves obtained under different operating conditions over aging time.

C. Dynamic Time Warping

Dynamic Time Warping (*DTW*) is well-known technique for measuring similarity between two time-dependent sequences that might vary in speed. It has been first developed for speech recognition [8] and then successfully used in other domain such as data mining where it was used as a metric to replace the Euclidian distance [10]. The interest of such a technique is to take into account the possible shifting and distortion between to signals. Over the years, the weaknesses of the algorithm in terms of complexity and scale adaptability have been answered to make the DTW more reliable [12].

Let $X = (x_1, x_2, \ldots, x_N)$ and $Y = (y_1, y_2, \ldots, y_M)$ be 2 sequences of respective size N and M. The purpose of the DTW algorithm is to find the optimal match between the points of X and Y. This is done by computing first the accumulative cost matrix $C = [c_{ij}]$ of size $N \times M$ where each element c_{ij} represents the minimum accumulative error between x_i and y_j. This is achieved recursively according to eq. (1).

$$c_{ij} = d(x_i, y_j) + min(c_{i-1,j-1}; c_{i-1,j}; c_{i,j-1}) \quad (1)$$

In this equation, $d(x_i, y_j)$ is the distance between x_i and y_j. This distance is calculated as expressed in eq. (2). Here, the error between the derivative at instant i and j is also taken into account, where ∂x_i and ∂y_j are the derivative of X and Y at instant i and j respectively.

$$d(x_i, y_j) = |x_i - y_j| + |\partial x_i - \partial y_j| \quad (2)$$

In order to increase the computation time, only the points in the "Sakoe-Chiba band" are computed [8]. This means that the warping path is looked up in a window w around the diagonal $i = j$. Once the cost matrix C has been computed, the optimal warping path $p = (p_1, p_2, \ldots, p_L)$ with $p_k = (i, j) \in [1..N] \times [1..M]$ giving the correspondence between each elements x_i and y_j of both sequences is built following 3 criteria:

- Boundaries: the first and the last points of the warping path are the first and last points of the sequences.
- Monotonicity: the path points p_k are set by increasing order of i and j.
- Step size: from p_k to p_{k+1}, i and j can not be increased of more than 1.

The optimal warping path computation is detailed in algorithm 1.

Fig. 2 shows an example of the obtained matching between 2 EIS curves. Both EIS curves were obtained on the same fuel cell for different current conditions. The blue and red curves were recorded at two different current densities. The dotted lines display the corresponding points.

It seems obvious from Fig. 2 that the obtained matching between the 2 curves is coherent. In particular, it can be noticed that the local minimum and maxima are correctly matched. From this match, it is now possible to compute the distance along $Re(Z)$ and along $Im(Z)$. These distances are respectively noted $DistX$ and $DistY$ in the following. Fig. 3 displays both $DistX$ and $DistY$ for the example shown in Fig. 2. In this figure, the distance is presented depending on the path index but it could also be displayed depending on the EIS frequencies. Here, the blue curve is used as the reference.

The analysis of distance curves displayed in Fig. 3 is consistent with the observations that can be made on Fig. 2. Along $Re(Z)$, one can notice that the matching points are very near till the first maximum where they start being shifted. This shifting stabilizes after the local minimum. This is exactly the evolution that is described by $DistX$. It is first very close to 0, then increases until it stabilizes. The same observation can be made on $Im(Z)$. The matching points are very close till the first maximum where the red curve is higher than the blue one. The level of the 2 curves are similar again around the local minimum and then the red curve becomes lower than the blue one before reaching the same level again. This evolution is well depicted by $DistY$ which is almost constant around 0, then shows an increase,

Algorithm 1 Optimal Warping Path

```
p = (N, M)
i = N, j = M
while (i > 1) and (j > 1) do
  if i == 1 then
    j = j − 1
  else if j == 1 then
    i = i − 1
  else
    m = min(c_{i−1,j−1}; c_{i−1,j}; c_{i,j−1})
    if m == c_{i−1,j} then
      i = i − 1
    else if m == c_{i,j−1} then
      j = j − 1
    else
      i = i − 1, j = j − 1
    end if
  end if
  p = ((i, j); p)
end while
```

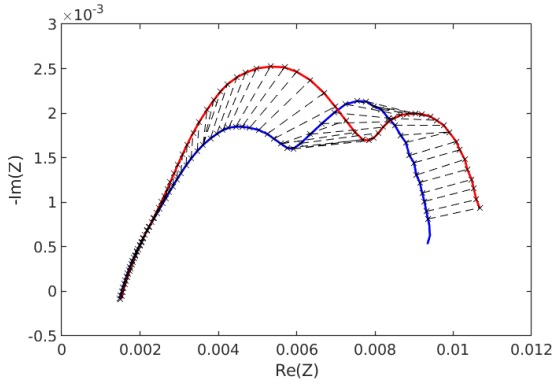

Figure 2. Example of DTW matching for 2 EIS curves.

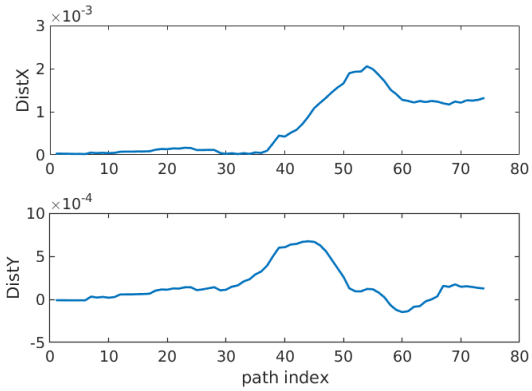

Figure 3. Distances $DistX$ and $DistY$ for the example given in Fig. 2.

goes back to 0, and then describes a decrease before going back to 0 again.

This example demonstrates that the DTW can be a powerful tool to describes the visual comparison that can be made between 2 curves.

III. Results and Discussions

A. Evaluation process

The DTW method is applied on the EIS extracted from the experimental data presented in II-B. These EIS curves are depicted in Fig. 4.

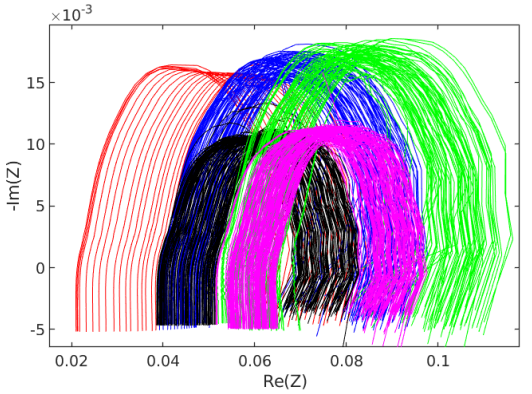

Figure 4. EIS curves from the experimental data campaign.

It can be observed in Fig. 4 that it seems to be 5 groups of EIS curves. To differentiate them, these groups have been plotted with 5 different colors: blue, red, black, magenta and green. From the FC perspective, these 5 groups are corresponding to different experimental conditions:

- Red (1): Break-in period of the FC (*BI*).
- Blue (2): SU/SD protocol 1, EIS are performed before the temperature is stabilized (*P1u*).
- Black (3): SU/SD protocol 1, EIS are performed after the temperature is stabilized (*P1s*).
- Green (4): SU/SD protocol 2, EIS are performed before the temperature is stabilized (*P2u*).
- Magenta (5): SU/SD protocol 2, EIS are performed after the temperature is stabilized (*P2s*).

It should be noted that if three temporal phases can be distinguished depending on wether the characterization is carried out during break-in, first or the second cycle of SU/SD, there is no predetermined order in the sequence of EIS within the same SU/SD cycle. From a temporal point of view, the datasets colored in black and blue in Fig. 4 (respectively green and red) are completely mixed.

The proposed method is evaluated on its ability to classify the 5 groups that were visually identified. To do so, the average absolute distances $mean(|DistX|)$ and $mean(|DistY|)$ are computed from the results of the DTW algorithm on each curve. Then, an unsupervised classification algorithm is performed on $mean(|DistX|)$ and $mean(|DistY|)$. The classification algorithm used here is a classic k-means clustering with 5 classes [13]. This algorithm was chosen for its simplicity. This choice will not be discussed furthermore in the paper.

B. Classification results

The results of the classification is displayed on Fig. 5. It can be seen in this figure that 5 groups are identified. The colors used in this figure are the same as in Fig. 4.

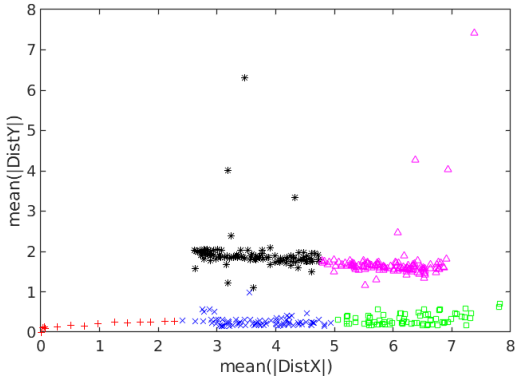

Figure 5. Classification results on the average distances of the DTW results on the EIS curves.

From Fig. 5, one can notice that the classes identified seem to match the visually identified groups. The first EIS (the one the more on the left in 4) is taken as the reference. The red crosses are very close to 0 and then shift to the right with almost no change on $mean(|DistY|)$. It is the same behavior for the red EIS observed in 4. Then, another class is identified as the blue crosses, characterized by a shifting on the $mean(|DistX|)$ axis and a tiny increase on $mean(|DistY|)$, which is what is observed on the blue EIS curves: they are shifted on the $Re(Z)$ axis with a slight increase on amplitude. On the right of the blue crosses class comes the green squares class with still a shifting on the right and a small increase on $mean(|DistY|)$, which is once again similar to one can observe on the green EIS curves. Concerning the black EIS curves, their position is similar

to the blue ones on the $Re(Z)$ axis but their amplitude is highly decreased. On Fig. 5, the black stars class have above the blue crosses one, showing a similar distance on $Re(Z)$ but more distance on $-Im(Z)$. The fact that an increase is observed on $mean(|DistY|)$ is due to the absolute operator that is used to compute the distance. However, it indicates an important change in amplitude which is the case here. The same observations can be done on the magenta triangles class compared to the green squares one.

The joined analysis of the EIS curves and the classification on the DTW distances demonstrates that DTW is a very interesting tools to transcript the observations one can visually make.

Table II presents the confusion matrix of the classification. A performance of 92.2% correct classifications is reached.

Table II
CONFUSION MATRIX OF THE EIS CURVES CLASSIFICATION.

		Target				
		BI	*P1u*	*P1s*	*P2u*	*P2s*
Output	*BI*	**14**	0	0	0	0
	P1u	19	**59**	0	0	0
	P1s	0	0	**105**	0	0
	P2u	0	8	0	**64**	0
	P2s	0	0	3	0	**111**
Rate		42.4%	88.1%	97.2%	100%	100%

The classification rates are very good except for Class BI where only 42.4% are correctly classified. Moreover, misclassified EIS curves are the one on the boundary to another class (BI to P1u, P1u to P2u, and P1s to P2s). As an example, Fig. 6 displays the EIS curves of Class BI (red) and the beginning of Class P1u (blue).

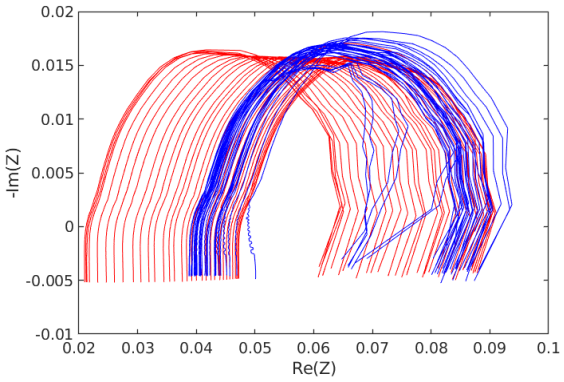

Figure 6. EIS curves of Class BI (red) and the beginning of Class P1u (blue).

It can be noticed from Fig. 6 that the first EIS curves in Class P1u are mixed up with some EIS curves of Class BI. As a consequence it is difficult to separate them visually which explains why the proposed method does not achieve to separate them and class them correctly.

C. Experimental data analysis

EIS is a interesting measure on FC because it gives information on the FC performance [14]. It is achieved in particular through the tracking of the ohmic resistance R_{HF} that can be extracted when the EIS crosses the $Re(Z)$ axis at high frequency, *i.e.* on the left of the curve. The lower this resistance, the better performance of the FC [15]. The R_{HF} is extracted from the different EIS curves and displayed in Fig. 7 according the classification results presented in section III-B, using the same colors as previously. For confidentiality reasons, normalized values are presented here.

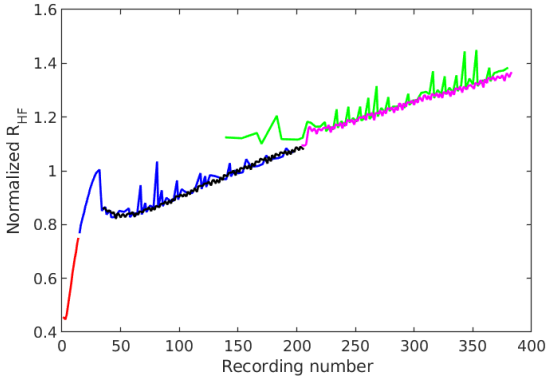

Figure 7. Normalized R_{HF} extracted from the EIS curves according their class (1: BI, 2: P1u, 3: P1s, 4: P2u, 5: P2s).

First, one can remark that the end of the break-in phase (Class 1 - first 33 recordings) have been misclassified, as mentioned in the previous section. From a global point of view, R_{HF} increases of about 50% along the 2 SU/SD phases (from recording 34 till the end), which represents about 120 h. This fact indicates that the conditions imposed to the FC had a strong impact on the performance in terms of electrical charge transfers.

More specifically, the analysis of R_{HF} during the 2 SU/SD phases shows that R_{HF} is more stable when the temperature is stabilized (black and magenta curves) as R_{HF} values fluctuates more on the blue and the green curves. This underlines the major influence of the temperature on the R_{HF}.

It is interesting to notice that the method was able to classify the EIS curves when the temperature was stable which are more interesting to exploit. Studying the trend of the black and the magenta curves shows indeed that the performance decrease is not the same for the 2 SU/SD strategies. The slope of each curve (black and magenta) was fitted as a first order polynomial. The computed values are displayed in table III.

Table III
SLOPE OF THE R_{HF} EVOLUTION IN STABILIZED TEMPERATURE CONDITIONS.

P1s	**P2s**
+ 0.0027	+ 0.0021

Tab. III confirms that the slope is lower in the case of P2 (magenta) than for P1, which would indicate that P2 is less degrading than P1. This result is quite surprising considering that the P1 protocol is supposed to be more careful with the FC. This result should indeed be studied more deeply to determine if this difference is really due to the change of SU/SD strategy and is linked neither to the general impact of cycling nor specific to a component aging of the FC prototype used. The strong degradation of the R_{HF} is indeed also an indicator of bipolar plates corrosion, which could explain the trend observed.

IV. Conclusions

With the consideration of a significant development of hydrogen technologies and an increase in research work, the development of relevant analysis tools is more useful than ever. As part of the aging monitoring of HT-PEM FC subjected to repeated start-stop cycles, numerous EIS data were generated. The method without a-priori presented in this article is an efficient way to classify Nyquist plots based on shape evolution recognitions.

A method based on Dynamic Time Warping was presented for the automated analysis of EIS curves. This method allows getting a measure of similitude between 2 curves. This method was evaluated on data from a high-temperature PEM Fuel Cell under 2 different conditions of Start & Stop cycling. The database represents 120 h of working.

The proposed method has proven to be efficient to give numerical indications that confirm the visual observations made on the different curves. The mean distance on $Re(Z)$ and $-Im(Z)$ resulting from the proposed method were used for unsupervised classification of the EIS curves using a classic k-means classifier. The proposed method reaches 92% correct classifications on 383 EIS curves and the misclassified curves are mainly the ones that were not possible to visually distinguish.

From this classification, R_{HF} was extracted from the different EIS curves. The DTW-based classification allowed separating the temperature stabilized and unstabilized EIS curves, which enlightened the impact of temperature on the quality of the R_{HF} extraction. Moreover, the R_{HF} analysis seems to fully benefit from this information.

However, work remains to be done in order to validate the method with new EIS data from the end of the presented aging campaign and from other campaigns on different fuel cell and with other operating conditions. To another extent, the method could be used for on-line diagnosis as EIS can be done during fuel cell operation and the automated analysis can detect degradation signatures.

Acknowledgment

This work is part of PIPAA project, included in HyPort meta-project, in partnership with Safran Power Units and financed by BPI France. The authors are very grateful to all the actors at the Hydrogen platform in Toulouse and at Safran Power Units who contributed to get these results.

References

[1] J. W. Pratt, L. E. Klebanoff, K. Munoz-Ramos, A. A. Akhil, D. B. Curgus, and B. L. Schenkman, "Proton exchange membrane fuel cells for electrical power generation on-board commercial airplanes," *Applied Energy*, vol. 101, pp. 776–796, 2013.

[2] International Energy Agency, "Global energy and co2 status report 2018," Energy Demand, Tech. Rep., 2018.

[3] S. S. Araya, F. Zhou, V. Liso, S. L. Sahlin, J. R. Vang, S. Thomas, X. Gao, C. Jeppesen, and S. K. Kær, "A comprehensive review of pbi-based high temperature pem fuel cells," *International Journal of Hydrogen Energy*, vol. 41, no. 46, pp. 21 310–21 344, 2016.

[4] L. Wang, A. Husar, T. Zhou, and H. Liu, "A parametric study of pem fuel cell performances," *International Journal of Hydrogen Energy*, vol. 28, no. 11, pp. 1263–1272, 2003.

[5] T. Génevé, C. Turpin, J. Régnier, O. Rallières, O. Verdu, A. Rakotondrainibe, and K. Lombard, "Voltammetric methods for hydrogen crossover diagnosis in a pemfc stack," *Fuel Cells*, vol. 17, no. 2, pp. 210–216, 2017.

[6] Z. Tang, Q.-A. Huang, Y.-J. Wang, F. Zhang, W. Li, A. Li, L. Zhang, and J. Zhang, "Recent progress in the use of electrochemical impedance spectroscopy for the measurement, monitoring, diagnosis and optimization of proton exchange membrane fuel cell performance," *Journal of Power Sources*, vol. 468, p. 228361, 2020.

[7] M. Tognan, C. Turpin, O. Rallières, O. Verdu, K. Lombard, and A. Rakotondrainibe, "Analyse et modélisation du vieillissement d'un stack de pile à combustible pem h2/o2." in *Symposium de Genie Electrique*, Grenoble, France, Jun. 2016.

[8] H. Sakoe and S. Chiba, "Dynamic programming algorithm optimization for spoken word recognition," *IEEE Transactions on Acoustics, Speech, and Signal Processing*, vol. 26, no. 1, pp. 43–49, 1978.

[9] Y. Permanasari, E. H. Harahap, and E. P. Ali, "Speech recognition using dynamic time warping (DTW)," *Journal of Physics: Conference Series*, vol. 1366, p. 012091, nov 2019.

[10] E. J. Keogh and M. J. Pazzani, "Scaling up dynamic time warping for datamining applications," in *Proceedings of the Sixth ACM SIGKDD International Conference on Knowledge Discovery and Data Mining*, 2000, p. 285–289.

[11] H. Li, "Time works well: Dynamic time warping based on time weighting for time series data mining," *Information Sciences*, vol. 547, pp. 592–608, 2021.

[12] S. Salvador and P. Chan, "Toward accurate dynamic time warping in linear time and space," *Intell. Data Anal.*, vol. 11, no. 5, p. 561–580, Oct. 2007.

[13] A. Likas, N. Vlassis, and J. J. Verbeek, "The global k-means clustering algorithm," *Pattern Recognition*, vol. 36, no. 2, pp. 451–461, 2003.

[14] K. Cooper and M. Smith, "Electrical test methods for on-line fuel cell ohmic resistance measurement," *Journal of Power Sources*, vol. 160, no. 2, pp. 1088–1095, 2006.

[15] X. Yuan, J. C. Sun, M. Blanco, H. Wang, J. Zhang, and D. P. Wilkinson, "Ac impedance diagnosis of a 500w pem fuel cell stack: Part i: Stack impedance," *Journal of Power Sources*, vol. 161, no. 2, pp. 920–928, 2006.